Journal of Applied Polymer Science

WILEY

Applied Polymer SCIENCE

RESEARCH ARTICLE

Hollow Glass Sphere Modification Effect on Mechanical Properties of Powder Bed Fusion Processed Polyamide 12 Parts

Mustafa Cüneyt Coşkun[1] | Alp Alparslan[1] | Umut Can Cingöz[2] | Mert Coşkun[2] | Burçin Özbay Kısasöz[3] | Ebubekir Koç[2,4] | İhsan Murat Kuşoğlu[5]

[1]SOCAR Türkiye Ar-Ge and Innovation, Izmir, Turkey | [2]Aluminium Test Training and Research Center (ALUTEAM), Fatih Sultan Mehmet Vakif University, Istanbul, Turkey | [3]Department of Metallurgical and Materials Engineering, Yildiz Technical University, Istanbul, Turkey | [4]Department of Industrial Engineering, Boğaziçi University, Istanbul, Turkey | [5]Meyer-Schwickerath-Str, Essen, Germany

Correspondence: Burçin Özbay Kısasöz (burcinozbay@gmail.com)

Received: 22 May 2025 | **Revised:** 6 September 2025 | **Accepted:** 7 September 2025

Funding: This work was supported by the Türkiye Bilimsel ve Teknolojik Araştırma Kurumu (3219504).

Keywords: additive manufacturing | composites | mechanical properties | polyamides | polymer | selective laser sintering

ABSTRACT

This study investigates the effects of modifying PA12 powder with a low concentration of surface-functionalized hollow glass spheres on powder characteristics and the mechanical properties of the Powder Bed Fusion–Laser Beam (PBF-LB) produced parts. A novel and scalable feedstock formulation was developed using a dissolution-precipitation method followed by dry mixing, which enabled the uniform incorporation of hollow glass spheres (Glass Beads (GBs)) while preserving the powder's flowability and thermal behavior. The powders were characterized by morphology, particle size distribution, flowability, melt behavior, and sintering window. After PBF-LB processing, the as-built parts were analyzed for part density, surface roughness, tensile, flexural, and impact properties. Results indicate that GB modification did not adversely affect powder quality but altered the mechanical performance of printed parts. 1 wt.% glass bead modified PA12 parts exhibited lower relative density and tensile strength compared to virgin PA12, but showed significantly enhanced impact resistance. This improvement is attributed to energy-absorbing mechanisms enabled by strong interfacial bonding between the glass beads and the PA12 matrix. This work introduces a novel toughening strategy for PBF-LB polymers, contributing a new material design pathway for producing lightweight, impact-resistant components in additive manufacturing for aerospace, automotive, and consumer applications using PBF-LB processes.

1 | Introduction

Powder bed fusion (PBF) is one of the seven categories of additive manufacturing (AM) processes [1] and a sophisticated process that involves the selective fusion of powder materials using thermal energy. This technique allows for the fusion of various substances, including metal powders, polymer powders, and alloys. The fusion process can be executed using multiple technologies, including lasers, electron beams, heated thermal printheads, or concentrated light sources combined with masks. Each method is chosen based on the specific requirements of the application [2–4]. Among these methods, PBF using a laser beam (PBF-LB) stands out as a technique suitable for mass production, which has progressed in the standardization and industrialization of the process. PBF-LB operates by selectively sintering polymer powders with a laser. The individual powder particles are joined through melting rather than fusion. This technology is advantageous for mass-producing products made

from a single material [5]. The process involves depositing a fine layer of powder, typically measuring 0.1 mm in thickness, onto a substrate. Subsequently, a laser beam is directed onto the platform to sinter the powder in designated regions selectively. This method facilitates the creation of precise and intricate geometries through controlled thermal interaction.

Although PBF-LB has established itself in polymer production methods, it is currently used in the industry for a limited number of polymer types, primarily due to the initial raw material being powder. Polymer powders are used mainly in the PBF-LB process, particularly in Selective Laser Sintering (SLS). And powders, depending on their type, are produced by emulsion/suspension polymerization, precipitation from solutions, milling and mechanical grinding, coextrusion, and other techniques such as spray drying and drop extrusion [6, 7]. The polymers commonly utilized in these powder processing technologies are mainly semicrystalline thermoplastics. However, there is also the option to use amorphous thermoplastics, bisegmented thermoplastics, or elastomers [8]. According to the Wohlers Report, polymers constitute the largest and most diverse group of materials used in AM. Polymers comprise 85.5% of the materials employed in AM technologies, whereas metals represent 11.5% [9]. The most frequently used polymer powders include polyamide powders, especially Polyamide 12 (PA12), along with PA11 and PA6 to a lesser degree [10]. Furthermore, this method also employs polystyrene (PS) powders, thermoplastic elastomers (TPEs), and polyaryletherketones (PAEKs), etc. [11–13]. PA12, as it provides the best performance, accounts for as much as 90% of the market share [14, 15]. This is due to the relatively reasonable price of these powders and the good repeatability obtained when using them in the AM process.

PA possesses superior attributes that make it particularly suitable for the PBF-LB process. PA12 powder is the predominant polymer utilized in this additive manufacturing process, mainly due to its extensive thermal range. This is especially significant in relation to the temperature differential between the initial phases of melting and crystallization. This unique characteristic enhances the processability and performance of PA in PBF-LB applications [16]. This family of materials is often preferred due to its advantageous thermal properties. Furthermore, PA demonstrates biocompatibility, along with commendable mechanical properties and high chemical stability, making it suitable for various applications. Despite its low density, approximately 1 g/cm^3, PA exhibits remarkable resistance to impact, particularly in dry or cold conditions, and possesses outstanding bending and fatigue strength [17–20]. Further, in the Powder Bed Fusion-Laser Beam (PBF-LB) processing of Polyamide 12 (PA12), various micro- and nano-scale materials have been incorporated into the powder feedstocks [21–25] to tailor the properties of the final parts. These fillers serve to enhance and improve thermal stability [26], mechanical strength [27], electrical conductivity [28], and antibacterial response [29], depending on the intended application. Inorganic fillers, such as silica (SiO_2) and alumina (Al_2O_3), are frequently used to enhance dimensional stability, optical properties, and stiffness [30, 31]. Carbon-based fillers, including carbon black, carbon nanotubes (CNTs), and graphene, are introduced to impart electrical conductivity and mechanical reinforcement [32–34], although their dispersion and laser interaction require careful control. Metallic powders, such as aluminum and copper, are added to hybrid applications to enhance thermal or electrical performance [35, 36]. For biocompatible or medical applications, bio-ceramic fillers, such as hydroxyapatite, are explored to enhance bioactivity, while antimicrobial nanoparticles, including silver or zinc oxide, provide hygienic functionality [37, 38]. Additionally, ceramic nanoparticles, such as titanium dioxide, are employed for UV stability and improved abrasion resistance [39, 40]. The selection and surface modification of these fillers are crucial, as they must be compatible with the PA12 matrix and PBF-LB processing parameters to avoid compromising powder flowability, sintering behavior, and final part integrity.

Glass beads are one of the microparticle modifiers, not only for PBF-LB processed PA12 [23, 41, 42] but also for other polymer types, such as Polyetherketone (PEK) [43] and Polypropylene (PP) [44], to prevent warping during PBF-LB processing and inhibit crack propagation, thereby improving the toughness of as-built parts under mechanical loads. Studies with glass bead modification have shown that using a coated glass bead, i.e., one with an amino silane group, forms a strong covalent bond through the reaction of the amino group of the silane with the carboxyl group of the polyamide chain, further improving the filler-matrix adhesion and the toughness of the parts [45]. The above studies investigated high loading amounts (ranging from 5 to 40 wt.%) of glass beads in the PA12 matrix and found that increasing the glass bead amount reduces both the tensile strength and impact resistance. Compared to literature, this study primarily focuses on investigating the low mixing amount (1 wt.%) of surface-coated hollow glass spheres, examining not only the mechanical properties of PBF-LB processed as-built parts but also the powder properties after dry mixing in comparison with dissolution-precipitated virgin PA12 powders. This work presents a novel toughening strategy for PA12 in laser-based additive manufacturing, utilizing minimal filler content with targeted surface modification. It provides a scalable, lightweight, and process-compatible solution for enhancing part toughness, distinguishing it from previous studies that focused on heavier loadings or unmodified fillers. In other words, this study demonstrates a previously unexplored impact strength enhancement strategy for PBF-LB polymers by incorporating surface-functionalized hollow glass spheres into PA12 powder at low concentrations. Compared to the literature, a low amount of glass bead modification (1 wt.%) in PBF-LB processed PA12 parts showed a mechanical trade-off. On the one hand, tensile and flexural strength decrease; on the other hand, elongation and impact toughness improved due to the energy mechanism. This trade-off makes glass bead-modified PA12 parts suitable for use in protective equipment and enclosures, as well as automotive interior components and consumer electronics housings, which require enhanced crack propagation resistance.

2 | Materials and Methods

2.1 | Materials

Virgin PA12 and hollow glass bead modified PA12 (GB-PA12) powder feedstocks are produced at SOCAR Refinery and Petrochemical Business Unit, Türkiye, following the dissolution-precipitation method using ethanol (min. 96% purity) and PA12-based granules (Grilamid L16 with a molecular

weight < 45,000 g/mol, EMS-Chemie AG) as starting materials, given in Figure 1. The obtained polyamide powder is separated from the solvent by centrifugation carried out at 600 rpm for 12 min with a Vibromak VKYA50. Collected precipitated PA12 powder feedstocks were ground using a double-blade grinder with a rotation speed of 28,000 rpm for 40 s, and sieved (> 32 μm and < 100 μm) to assess a suitable particle size distribution for the PBF-LB process. As an additive, micro-hollow glass spheres with a surface modified by amino functional groups are used, improving wettability and adhesion with the PA12 matrix. These spheres have an average particle diameter of 22 μm and a true density of 0.46 g/cm^3. 1 wt.% of glass bead modification, together with flow-enhancing agents such as nano-silica and other process-enhancing additives (in total < 3 wt.%), is mixed with as-produced PA12 powders using a 3D shaker mixer (Turbula, WAB AG) at 40 rpm for 30 min (Figure 1).

2.2 | Methods

2.2.1 | Powder Characterization

The properties of virgin and 1 wt. % GB-modified PA12 powder feedstock are evaluated extensively using several characterization techniques. Powder morphology and GB distribution within PA12 powders are observed by SEM (Hitachi-SU3500). The particle size distributions of both powders are measured using laser diffraction (Malvern Mastersizer, 2000). Melting and crystallization temperatures are measured using Differential Scanning Calorimetry (DSC-Shimadzu DSC-60 Plus) with a heating rate of 10°C/min to 250°C and a cooling rate of 10°C/min to room temperature, to determine the sintering window of the PBF-LB process. Moreover, the additive content of the mixture was verified through thermogravimetric analysis (TGA-TA Instruments SDT 650) with a heating rate of 20°C/min to 800°C.

The melt flow behavior of the powders is determined by using a melt flow index tester (Instron Ceast MF20) under a load of 2.16 kg at 235°C. The flow behavior of powders is determined by measuring the avalanche angle of powders using the rotating drum (Granudrum) and the Hausner ratio, as specified in ISO/ASTM 52925:2022 [46].

2.2.2 | PBF-LB Process of PA12-Based Powder Feedstocks

Virgin and GB-modified PA12 powder feedstocks are processed by the EOS P396 model PBF-LB machine to build density and mechanical test specimens shown in Figure 2. Each powder composition is processed with two different parameter sets, as shown in Table 1, which are the best experienced conditions of the authors for processing virgin PA12 powders. Both sets yielded the same volumetric energy density, which can be calculated using Equation (1). The powders are processed at a powder bed temperature of 170.5°C and a removal chamber temperature

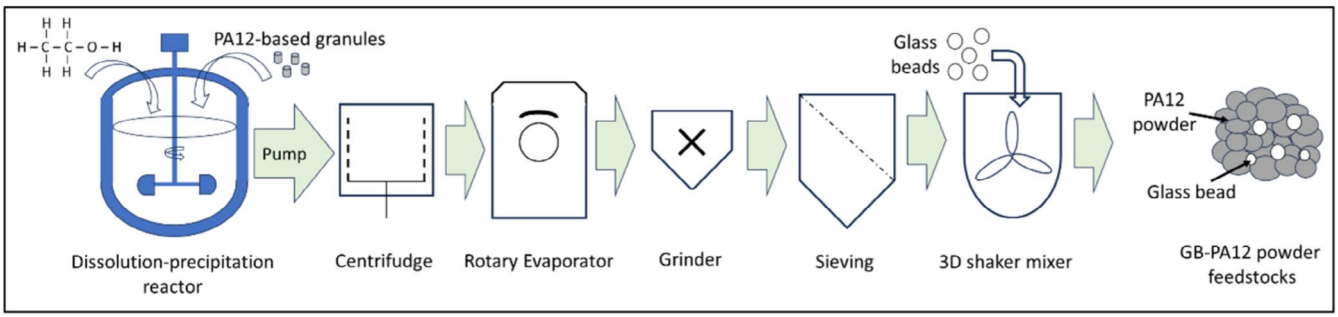

FIGURE 1 | Schematic illustration of virgin and glass bead modified PA12 powder feedstock production via dissolution-precipitation method. [Color figure can be viewed at wileyonlinelibrary.com]

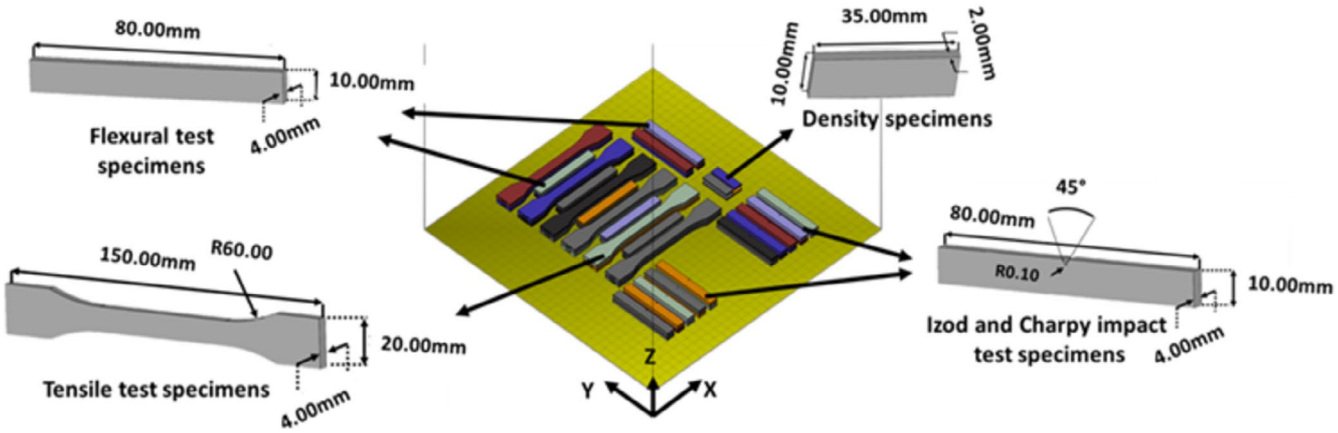

FIGURE 2 | Additive manufacturing file design of the build job to produce test specimens via the PBF-LB process and corresponding test sample dimensions. [Color figure can be viewed at wileyonlinelibrary.com]

TABLE 1 | PBF-LB process parameters for printing build jobs.

Process Set-ID	Laser power (P) (W)	Scanning speed (v) (mm/s)	Hatch distance (h) (mm)	Powder layer thickness (t) (μm)	Volumetric energy density (VED) (J/mm^3)
Set-1	20	5000	0.15	100	0.267
Set-2	21	3150	0.25	100	0.267

of 140.5°C, respectively, which are far below the softening temperature of the hollow glass spheres.

As-built parts' surfaces are blasted with glass beads before conducting corresponding tests for part characterization.

$$VED = \frac{P}{v \times h \times t}$$

2.2.3 | As-Built Parts Characterization

The density of as-built parts is measured on three replicas using the immersion method, as specified in ISO 1183-1:2019 [47]. The surface roughness was characterized by employing a Mitutoyo SJ-500 profilometer. The arithmetic mean roughness (Ra) values were quantified for both virgin PA12 samples and PA12 samples reinforced with 1 wt.% glass beads, which were fabricated under two distinct processing parameter sets. The tensile strength and elongation at break of as-built parts are determined by testing six replicas (Type 1B) per composition using an Instron 5966 universal test machine at a test rate of 5 mm/min, following the ISO 527-2 standard [48]. ISO 527 is comparable to ASTM D638, which is applicable for isotropic or mildly anisotropic plastics with low strengths (< 100 MPa). The flexural modulus of as-built parts is determined by testing six replicas per composition using an Instron 5966 universal test machine with a support span of 64 mm and a test rate of 2 mm/min, in accordance with the ISO 178 standard [49]. The Izod and Charpy impact strengths of as-built parts are determined by testing five samples per composition using an Instron Ceast 9050 universal test machine, following ISO 180 [50] and ISO 179 [51], respectively. The fracture surfaces of tensile and impact samples are examined using an SEM (Hitachi SU3500).

3 | Results and Discussion

3.1 | Properties of As-Produced Powder Feedstocks

The morphology of virgin PA12 powders produced via the dissolution-precipitation method and 1 wt.% GB modified PA12 powders is given in Figure 3. Virgin PA12 powder feedstocks have a spherical to potato shape morphology, as seen in Figure 3a,b. As shown by white arrows in Figure 3c,d, the glass beads (white spheres) are randomly distributed between the PA12 powders after modification.

Powder properties are evaluated to understand the effect of glass bead modification, as given in Table 2. Since the average particle size of glass beads was 22 μm, $D_{v,10}$ and $D_{v,50}$ fractions of GB-PA12 resulted in smaller size distributions than virgin PA12 powders. However, flow behavior is compared by considering the Hausner ratio and the Avalanche angle. On the one hand, measuring the Hausner ratio was not a suitable characterization technique to distinguish the effect of GB on flowability compared to the virgin ones. Still, both powders had good flowability with a Hausner ratio of 1.05 [10]. On the other hand, the rotating drum test was more precise in determining the effect of GB modification, and the results revealed that virgin PA12 has better flow behavior with a lower avalanche angle of 27°, which was better than the literature values [10]. Additionally, the GB modification did not adversely affect the melt flowability or sintering window, indicating that both powders can be processed under the same PBF-LB process parameter sets. Furthermore, the crystallinity of the GB-modified powders was almost 10% higher compared to the virgin PA12 powders.

Overall, the GB modification did not adversely affect the powder properties, except for a slight decrease in flowability, which can be attributed to the reduced particle size distribution resulting from the addition of glass beads having an average particle size of 22 μm.

However, according to TGA analysis results, the residue content at 800°C is approximately 3.2 wt.%, which complies with the total additive content, including nano-silica, other additives (excluding GB), and 1 wt.% GB.

3.2 | Macrostructural Properties of PBF-LB Processed Parts

Both powders are PBF-LB processed to produce mechanical test specimens under two different process parameter sets by applying the same VED of 0.267 J/mm^3, where Set-1 has a higher scanning speed of 5000 mm/s with a smaller hatch spacing of 150 μm, and Set-2 has a lower scanning speed of 3150 mm/s and a larger hatch spacing of 250 μm. The effects of two different process parameters on densification and surface roughness of both virgin and GB-modified samples are presented in Figure 4.

Virgin PA12 parts achieve a relative density of 95% under both sets 1 and 2 after PBF-LB processing (Figure 4a), which is higher than the literature values reported [10, 26]. However, GB-modified ones result in a very low relative density of 65%, which is slightly enhanced under Set-2 conditions by setting a lower scanning speed and wider hatch spacing during PBF-LB processing (Figure 4a). In addition to the GB density reduction effect, it can be said that the sinter voids formed within the structures to which additives were added also contribute to the decrease in density. But these values are still far below the reported values [10]. The slightly decreased flow behavior and smaller particle size distribution of GB-modified ones require a process parameter optimization different from that used for processing virgin PA12.

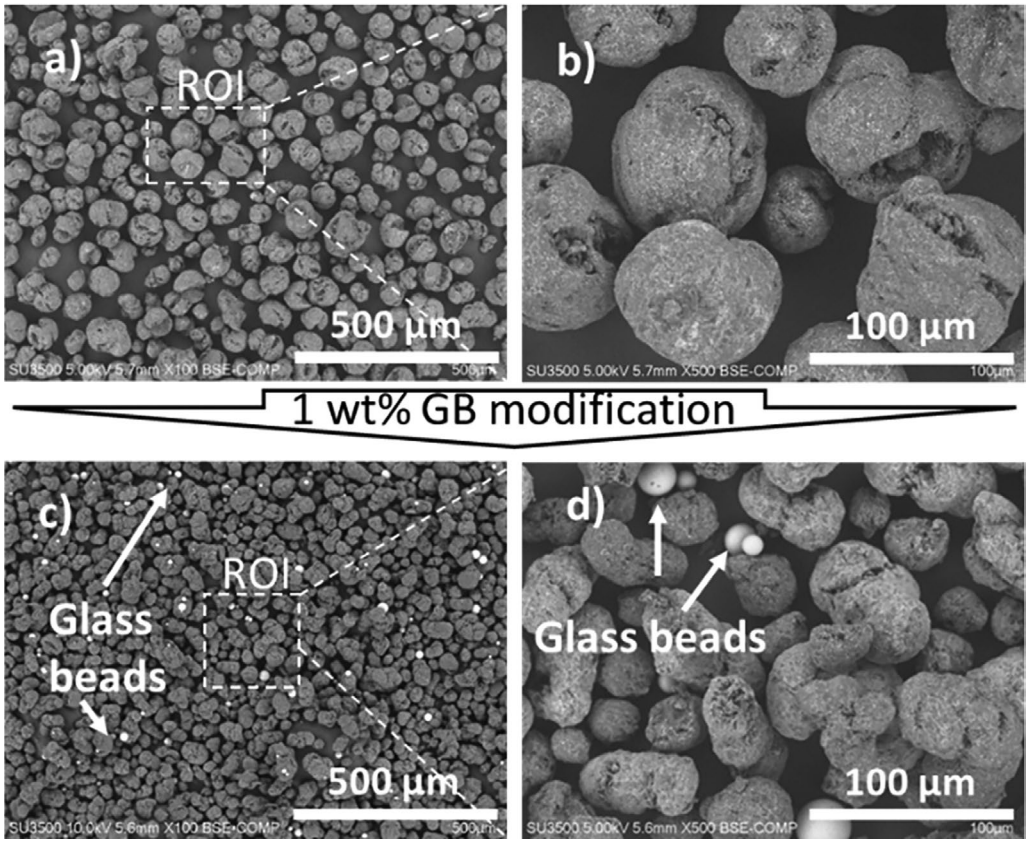

FIGURE 3 | SEM images of (a, b) virgin PA12 and (c, d) 1 wt.% glass bead modified PA12 powder feedstocks. White arrows indicate glass beads distributed between PA12 powders.

TABLE 2 | Properties of PA12 and GB-PA12 powder feedstock.

	Properties							
	Particle size distribution (µm)			Hausner ratio (–)	Avalanche angle (°)	MFI (g/10 min)	Sintering window (°C)	Crystallinity (%)
Materials	$D_{v,10}$	$D_{v,50}$	$D_{v,90}$					
PA12	50.2	73.0	105.7	1.05	26.8	43	23	37
GB-PA12	32.8	54.3	88.7	1.05	30.7	42	24	40

Additionally, the surface roughness of virgin and GB-modified ones can be seen in Figure 4b. Virgin PA12 parts exhibited a lower surface roughness (average 6.3 µm) under PBF-LB conditions of Set-2 compared to Set-1, where a lower scanning speed and wider hatch spacing are set. Furthermore, GB-modified ones exhibit higher surface roughness compared to virgin ones.

3.3 | Mechanical Properties of PBF-LB Processed Parts

3.3.1 | Tensile Properties

Figure 5 shows the tensile test results of as-built parts. Contrary to the literature values [10], virgin PA12 parts resulted in a very high average UTS of 67 MPa under Set-1, which increased to 71 MPa under Set-2 (Figure 5a). In comparison, GB-PA12 parts resulted in an average UTS of 42.5 MPa under Set-1 and increased to 47 MPa under Set-2 (Figure 5a). As expected, an increase in UTS decreases elongation, as shown in Figure 5b. GB-modified parts processed under Set-1 resulted in the highest elongation values of 15%. In contrast, it is around 7.5% for the PA12 ones. Compared to Set-2, higher scanning speed and smaller hatch spacing result in higher ductility in both material systems.

Figure 6a–c illustrate the tensile fracture surface of the PA12, while Figure 6d–f illustrate the fracture surface of the PA12-GB. According to Figure 6a,d, the fracture surface of the PA12 has a smoother structure, while the GB-reinforced composite has a rougher structure. Figure 6a–c show that the fracture occurred rapidly and sharply, with limited energy absorption via crack propagation. This results in a smooth fracture surface characterized by distinct patterns, forming a brittle fraction with limited energy absorption. In conjunction with the fracture surface images depicted in Figure 6b,c, the presence of a brittle fracture

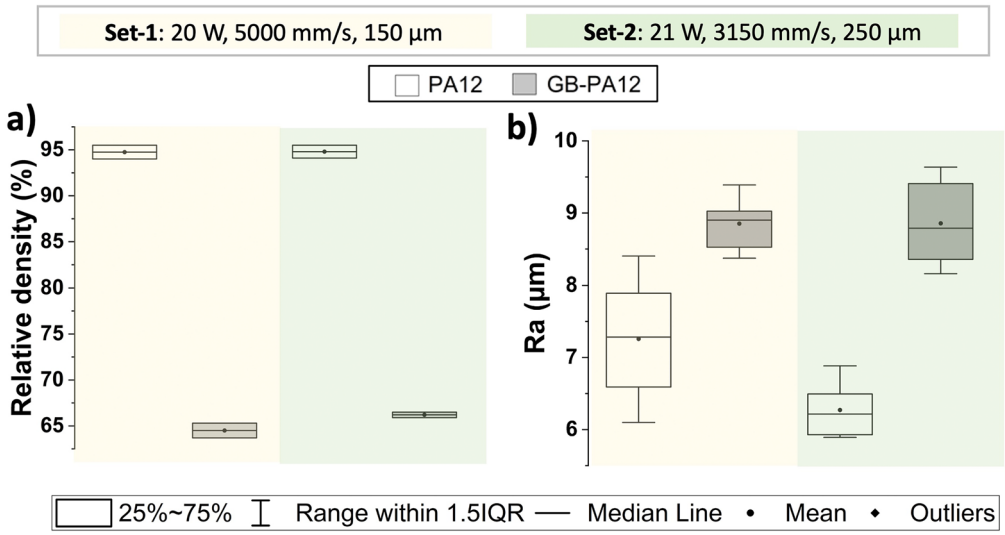

FIGURE 4 | (a) Relative density and (b) surface roughness of both virgin and GB-modified parts processed by PBF-LB under Set-1 (20 W, 5000 mm/s, 150 µm) and Set-2 (21 W, 3150 mm/s, 250 µm) conditions. [Color figure can be viewed at wileyonlinelibrary.com]

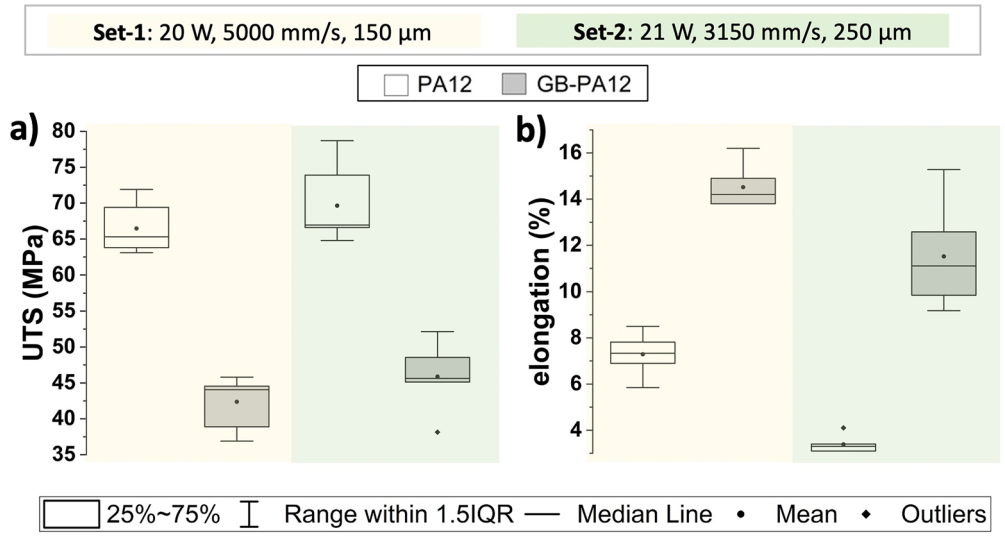

FIGURE 5 | (a) Ultimate tensile strength and (b) elongation of both virgin and GB-modified parts processed by PBF-LB under Set-1 (20 W, 5000 mm/s, 150 µm) and Set-2 (21 W, 3150 mm/s, 250 µm) conditions. [Color figure can be viewed at wileyonlinelibrary.com]

surface and brittle fracture paths, characterized by the predominance of normal stresses following the tensile test, is evident. A similar fracture mechanism for PBF-LB processed parts was also mentioned by Hooreweder et al. [52] and Rosso et al. [53].

As illustrated in Figure 6d, the glass bead (GB) modification exhibits a clear dispersion of the glass beads within the matrix. Moreover, the fracture surface consists of voids originating from glass beads and the tensile test effect. The voids occurring around the glass beads, as seen in Figure 6e,f, can be defined as sintering voids, which form during the PBF-LB process. Moreover, the voids observed on the fracture surface can be attributed to the ductile fracture of the PA12-GB structure. It is revealed that the glass beads form a barrier for crack propagation, and ductile fracture is observed in the PA12-GB sample. The stress resulting from the tensile test is concentrated around the bead, and sintering voids cause partial bonding gaps in the glass bead. Following the findings of Lui et al. [54] and Seltzer et al. [42], GBs can be regarded as spherical voids. Tensile stress is concentrated at the PA12-GB interface, leading to an improvement in fracture behavior. In regions where glass beads are present, fracture may be driven by an energy-absorbing mechanism. The crack paths became irregular due to the effect of the glass beads, resulting in a more complex fracture behavior, as the structure is composite. It was found that glass beads can aid energy absorption.

3.3.2 | Flexural Properties

Figure 7 illustrates the flexural strength and flexural modulus of parts, a crucial measure for structural components, automotive parts, or construction materials subjected to bending forces. The flexural strength of both materials (Figure 7a) indicates that Set-1 results in the highest strengths for both materials, with

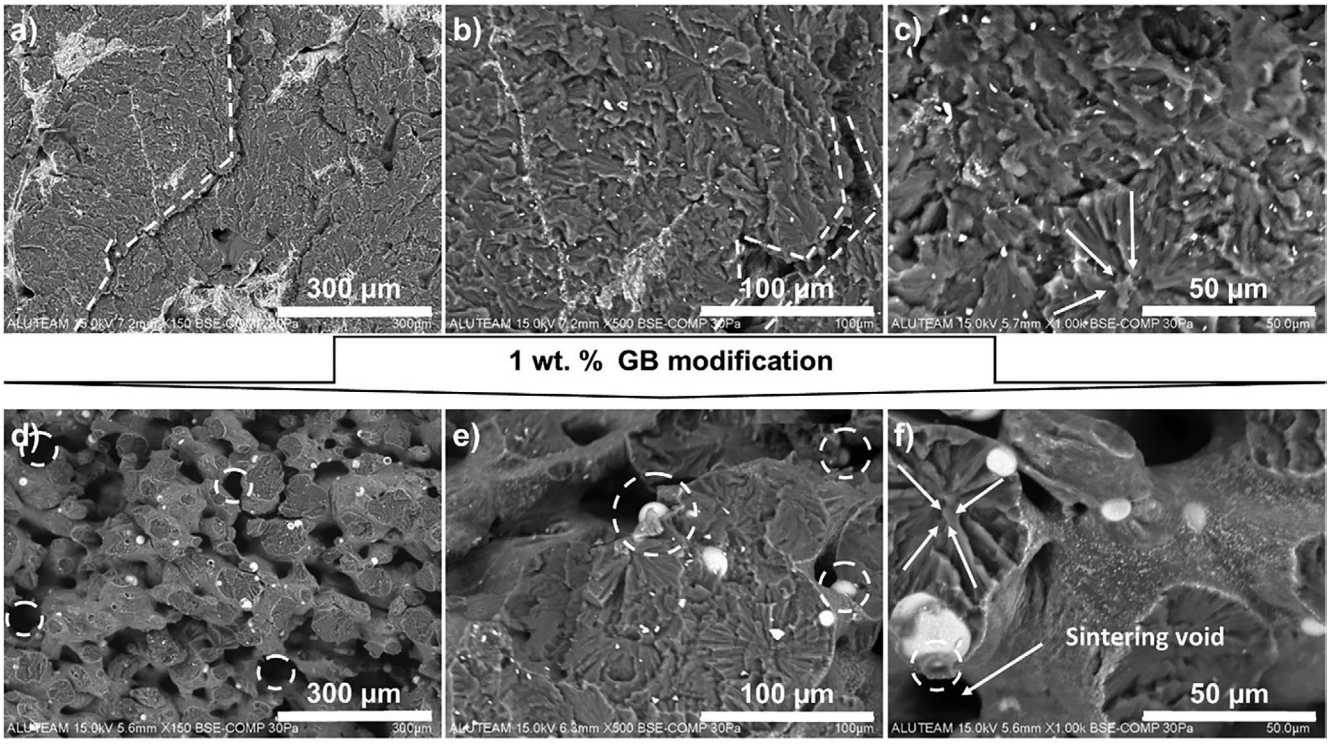

FIGURE 6 | Fracture surfaces of virgin PA12 (a–c) and 1 wt.% glass bead-modified PA12 (d–f) after tensile test.

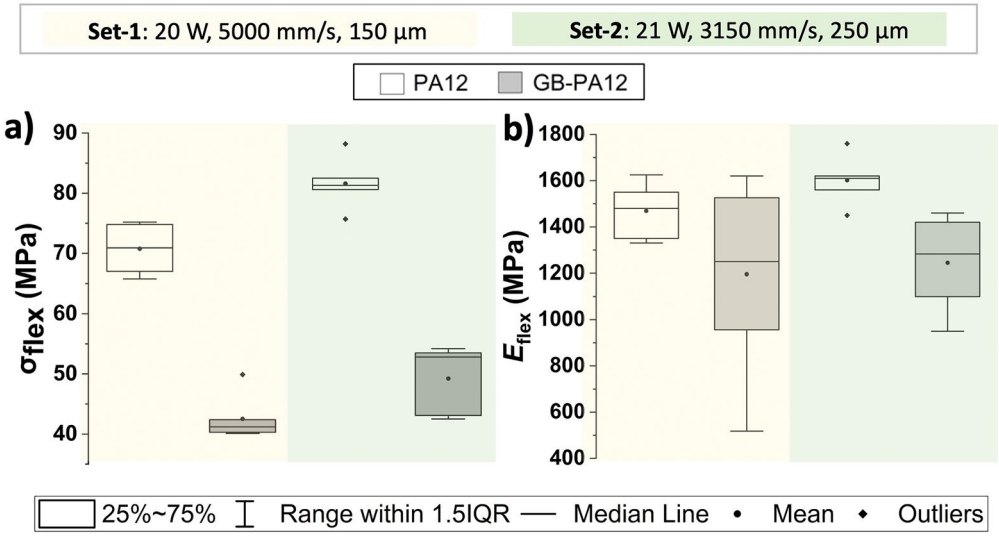

FIGURE 7 | (a) Flexural strength and (b) flexural modulus of both virgin and 1 wt.% GB-modified PA12 parts processed by PBF-LB under Set-1 (20 W, 5000 mm/s, 150 µm) and Set-2 (21 W, 3150 mm/s, 250 µm) processing conditions. [Color figure can be viewed at wileyonlinelibrary.com]

PA12 having the highest value of 80 MPa and GB-PA12 having a strength of 50 MPa. The flexural modulus of both virgin and GB-modified PA12 parts (Figure 7b) was higher under Set-2, with virgin PA12 resulting in 1600 MPa, which is 30% higher than that of the GB-PA12 parts.

3.3.3 | Impact Properties

The toughness and energy a polymer can absorb before breaking are determined by Izod (Figure 8a) and Charpy (Figure 8b) impact strengths, which are essential for parts where sudden forces or collisions might occur. Despite the other mechanical properties, both Izod and Charpy impact strengths were higher for GB-modified PA12 parts. The Izod impact strength of virgin PA12 parts was higher under Set-1 compared to Set-2, while it was higher for GB-PA12 parts processed under Set-2 compared to Set-1.

The fracture surfaces of virgin and GB-modified PA12 after the impact test are further evaluated by SEM (Figure 9) to understand the fracture mechanism better.

Figure 9 illustrates that SEM images show that the glass beads are dispersed within the PA12 matrix. However, sintering

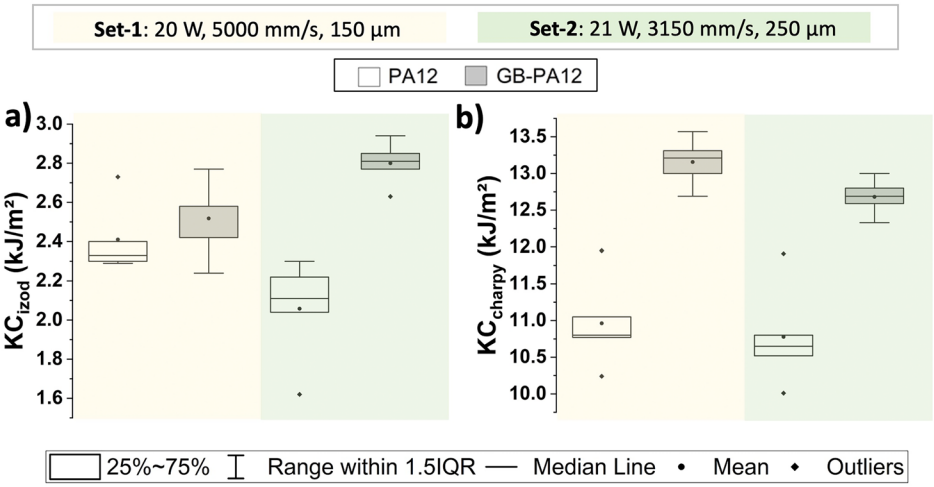

FIGURE 8 | (a) Izod impact strength and (b) Charpy impact strength of both virgin and 1 wt.% GB-modified parts processed by PBF-LB under Set-1 (20 W, 5000 mm/s, 150 µm) and Set-2 (21 W, 3150 mm/s, 250 µm) processing conditions. [Color figure can be viewed at wileyonlinelibrary.com]

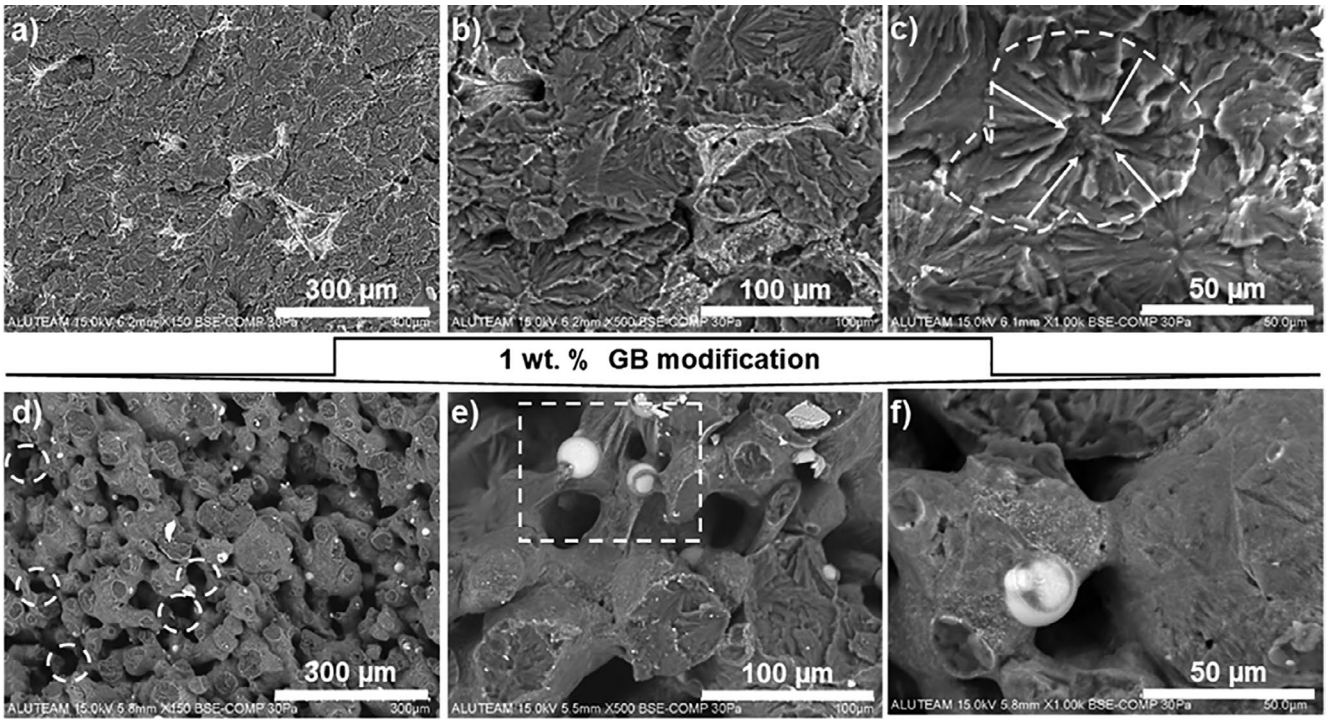

FIGURE 9 | Fracture surfaces of virgin PA12 (a–c) and 1 wt.% glass bead-modified PA12 (d–f) parts after impact test.

voids and partial bonding voids between the glass beads and the polymer matrix can be observed. These voids are likely a consequence of incomplete sintering across the material structure. The increased impact strength of PA12 depends on the uniform distribution of glass beads and improved interface. The beads can prevent material deformation from cracking by distributing stress intensity during the impact test. This can enhance the impact strength by increasing the material's energy absorption capacity [44, 45]. In particular, the wettability of the glass beads enabled them to be effectively embedded in the polymer, which contributed to an increase in the energy absorption capacity and enhanced the impact strength compared to virgin PA12. Nevertheless, this increase in mechanical properties is accompanied by the formation of ductile fracture. Additionally, Özbay Kısasöz et al. [55] noted that a higher amount of the hollow GB reduces the impact strength of the structure due to low interfacial bonding between the matrix and filler, as well as the heterogeneous distribution of the GB. However, this study reveals that a lower amount of GB has a beneficial influence on energy absorption, and the toughness of the structure can be enhanced by adding 1 wt.% GB.

Figure 10a displays the SEM image of the fracture surface of the virgin PA12 specimen, while Figure 10b depicts the fracture surface of the PA12 specimen reinforced with glass beads. As illustrated in Figure 10a, the fracture surface of the virgin PA12 exhibits a predominantly brittle fracture mode, characterized

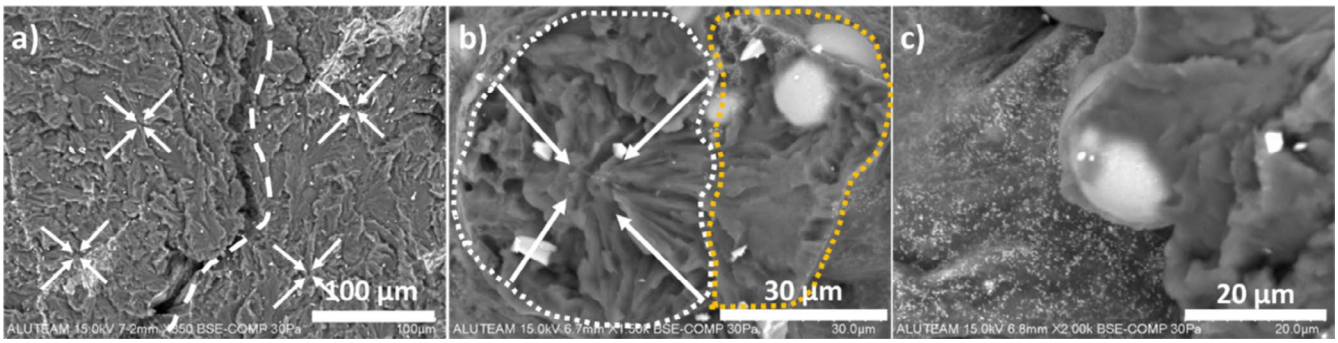

FIGURE 10 | Fracture surfaces of virgin PA12 (a) and 1 wt.% glass bead-modified PA12 (b, c). [Color figure can be viewed at wileyonlinelibrary.com]

by observable crack propagation paths that converge at specific points, indicating low energy absorption during the failure process. Conversely, Figure 10b suggests that in regions devoid of glass beads, the fracture maintains a brittle and continuous path, which tends to localize at particular points. However, in areas containing glass beads, a comparatively deformed fracture surface is apparent. Additionally, the type of fracture surface suggests that the presence of glass beads alters the crack propagation mechanism, leading to more uniform and potentially more elastic fracture behavior. These observations indicate that the integration of glass beads enhances the alteration of fracture properties in PA12, thereby reducing the likelihood of brittle fracture.

Figure 10c illustrates a high-magnification SEM image emphasizing the interface between the glass bead and the PA12 matrix. The image distinctly demonstrates that the glass beads are effectively integrated into the polymer matrix, with no observable interfacial voids or debonding. This observation signifies good wetting and robust interfacial adhesion, which optimizes load transfer efficiency. Such a well-bonded interface is also anticipated to enhance the fracture behavior by hindering crack propagation and augmenting toughness.

4 | Conclusion

This study evaluated the influence of incorporating 1 wt.% aminosilane-modified hollow glass spheres into PA12 powder feedstocks for use in the Powder Bed Fusion-Laser Beam (PBF-LB) process. Powder characterization revealed that the addition of glass beads had a minimal impact on key thermal properties, such as the sintering window and melt flow behavior, thereby maintaining compatibility with standard PBF-LB process parameters. Although a slight reduction in flowability and part densification was observed, the overall processability of the modified powders remained suitable for additive manufacturing.

Mechanical testing revealed a clear trade-off between tensile properties and impact performance. While the GB-PA12 parts showed a reduction in ultimate tensile strength and flexural modulus compared to unmodified PA12, they exhibited significantly improved impact resistance. Notably, under Set-2 processing conditions, the flexural modulus increased by approximately 30%, from 1200 MPa for virgin PA12 to 1600 MPa with glass bead reinforcement. Scanning electron microscopy further confirmed that the embedded glass beads enhanced interfacial bonding and altered fracture behavior by impeding crack propagation and promoting more ductile failure modes.

Notably, SEM analysis confirmed that the presence of glass beads altered the fracture behavior by impeding crack propagation and promoting ductile failure, accompanied by improved wettability and adhesion. Furthermore, even setting the same VED, the materials' mechanical properties under different test conditions are highly dependent on processing strategies and should be considered to achieve the desired trade-off between properties.

Overall, this work introduces a novel toughening strategy for PA12 in PBF-LB by utilizing low-load, surface-functionalized hollow glass spheres. The findings suggest that even minimal filler content can be effectively used to tailor mechanical performance—particularly impact toughness—without compromising processability. This approach provides a scalable route for developing lightweight, durable components for applications where toughness is critical. Future studies should explore the optimization of glass bead content, alternative surface treatments, and their long-term effects on part integrity and durability.

Future studies will focus on the addition of a larger amount of glass beads (< 5 wt.%), glass bead sizes, and optimization of PBF-LB process parameters, while maintaining high part density. It is also recommended to investigate atomic-scale structural properties using a high-resolution transmission electron microscope to understand and gain a deeper understanding of the material's behavior under mechanical forces.

Author Contributions

Mustafa Cüneyt Coşkun: conceptualization (supporting), investigation (equal), methodology (lead), validation (lead), writing – original draft (supporting), writing – review and editing (equal). **Alp Alparslan:** methodology (supporting), project administration (lead), supervision (lead). **Umut Can Cingöz:** methodology (supporting), validation (equal), writing – original draft (equal), writing – review and editing (equal). **Mert Coşkun:** methodology (equal), validation (equal), writing – review and editing (equal). **Burçin Özbay Kısasöz:** conceptualization (lead), investigation (lead), methodology (lead), project administration (lead), supervision (equal), validation (lead), writing – original draft (lead), writing – review and editing (equal). **Ebubekir Koç:** project administration (equal), supervision (lead), writing – original draft (supporting), writing – review and editing (supporting). **İhsan Murat Kuşoğlu:** investigation (supporting), methodology (supporting),

validation (supporting), writing – original draft (lead), writing – review and editing (lead).

Acknowledgments

This study was supported by The Scientific and Technological Research Council of Türkiye (TÜBİTAK) under project number 3219504.

Conflicts of Interest

The authors declare no conflicts of interest.

Data Availability Statement

The data that support the findings of this study are available from the corresponding author upon reasonable request.

References

1. ISO/ASTM 52900:2021, Additive Manufacturing—General Principles—Terminology, 2025, https://www.iso.org/obp/ui/#iso:std:iso-astm:52900:ed-2:v1:en.

2. M. Kamran and A. Saxena, "A Comprehensive Study on 3D Printing Technology," *MIT International Journal of Mechanical Engineering* 6, no. 2 (2016): 63–69.

3. D. Bourell, J. P. Kruth, M. Leu, et al., "Materials for Additive Manufacturing," *CIRP Annals* 66 (2017): 659–681.

4. Y. Zhai, D. A. Lados, and J. L. Lagoy, "Additive Manufacturing: Making Imagination the Major Limitation," *Journal of Management* 66, no. 5 (2014): 808–816, https://doi.org/10.1007/s11837-014-0886-2.

5. T. Stichel, T. Brandl, T. Hauser, B. Geißler, and S. Roth, "Electrophotographic Multi-Material Powder Deposition for Additive Manufacturing," *Procedia CIRP* 74 (2018): 249–253.

6. M. Schmid, *Laser Sintering With Plastics* (Hanser, 2018).

7. J. Schmidt, M. Sachs, C. Blümel, et al., "A Novel Process Chain for the Production of Spherical SLS Polymer Powders With Good Flowability," *Procedia Engineering* 102 (2014): 550–556, https://doi.org/10.1016/j.proeng.2015.01.123.

8. S. Yuan, F. Shen, C. K. Chua, and K. Zhou, "Polymeric Composites for Powder-Based Additive Manufacturing: Materials and Applications," *Progress in Polymer Science* 91 (2019): 141–168, https://doi.org/10.1016/j.progpolymsci.2018.11.001.

9. T. Caffrey, T. Wohlers, and R. I. Campbell, *Executive Summary of the Wohlers Report* (Wohlers, 2016), 2019.

10. I. M. Kusoglu, S. Barcikowski, and B. Gökce, "Laser Powder Bed Fusion of Polymers: Quantitative Research Direction Indices," *Materials* 14, no. 5 (2021): 1169, https://doi.org/10.3390/ma14051169.

11. R. D. Goodridge, M. L. Shofner, R. J. M. Hague, et al., "Processing of a Polyamide-12/Carbon Nanofibre Composite by Laser Sintering," *Polymer Testing* 30, no. 1 (2011): 94–100, https://doi.org/10.1016/j.polymertesting.2010.09.011.

12. S. Greiner, K. Wudy, L. Lanzl, and D. Drummer, "Selective Laser Sintering of Polymer Blends: Bulk Properties and Process Behavior," *Polymer Testing* 64 (2017): 136–144, https://doi.org/10.1016/j.polymertesting.2017.09.018.

13. X. Gan, G. Fei, J. Wana, Z. Wang, M. Lavorgna, and H. Xia, *Powder Quality and Electrical Conductivity of Selective Laser Sintered Polymer Composite Components* (Woodhead Publishing Series in Composites Science and Engineering, 2020).

14. D. Drummer, M. Medina-Hernández, M. Drexler, and K. Wudy, "Polymer Powder Production for Laser Melting Through Immiscible Blends," *Procedia Engineering* 102 (2015): 1918–1925, https://doi.org/10.1016/j.proeng.2015.01.332.

15. H. Gu, F. AlFayez, T. Ahmed, and Z. Bashir, "Poly(Ethylene Terephthalate) Powder: A Versatile Material for Additive Manufacturing," *Polymers* 11, no. 12 (2019): 2041, https://doi.org/10.3390/polym11122041.

16. R. D. Goodridge, C. J. Tuck, and R. J. M. Hague, "Laser Sintering of Polyamides and Other Polymers," *Progress in Materials Science* 57, no. 2 (2012): 229–267, https://doi.org/10.1016/j.pmatsci.2011.04.001.

17. T. N. A. T. Rahim, A. M. Abdullah, H. M. Akil, D. Mohamad, and Z. A. Rajion, "Preparation and Characterization of a Newly Developed Polyamide Composite Utilising an Affordable 3D Printer," *Journal of Reinforced Plastics and Composites* 34, no. 19 (2015): 1628–1638, https://doi.org/10.1177/0731684415594692.

18. S. Kumar, R. Singh, T. P. Singh, and A. Batish, "Fused Filament Fabrication: A Comprehensive Review," *Journal of Thermoplastic Composite Materials* 36, no. 2 (2023): 794–814, https://doi.org/10.1177/0892705720970629.

19. B. Özbay, Manufacturing and Characterization of Polymer Composites by Using Selective Laser Sintering 3D Printing Method [PhD thesis]. Istanbul Technical University, Istanbul, 2021.

20. Omnexus, What Is Polyamide (Nylon)?,, 2018, https://omnexus.specialchem.com/selection-guide/polyamide-pa-nylon#.

21. T. Hupfeld, T. Laumer, T. Stichel, et al., "A New Approach to Coat PA12 Powders With Laser-Generated Nanoparticles for Selective Laser Sintering," *Procedia CIRP* 74 (2018): 244–248, https://doi.org/10.1016/j.procir.2018.08.103.

22. A. Al Rashid, S. A. Khan, S. G. Al-Ghamdi, and M. Koç, "Additive Manufacturing of Polymer Nanocomposites: Needs and Challenges in Materials, Processes, and Applications," *Journal of Materials Research and Technology* 14 (2021): 910–941, https://doi.org/10.1016/j.jmrt.2021.07.016.

23. A. J. Cano, A. Salazar, and J. Rodríguez, "Effect of Temperature on the Fracture Behavior of Polyamide 12 and Glass-Filled Polyamide 12 Processed by Selective Laser Sintering," *Engineering Fracture Mechanics* 203 (2018): 66–80, https://doi.org/10.1016/j.engfracmech.2018.07.035.

24. B. Sivadas, I. Ashcroft, A. Khlobystov, and R. Goodridge, "Laser Sintering of Polymer Nanocomposites," *Advanced Industrial and Engineering Polymer Research* 4, no. 4 (2021): 277–300, https://doi.org/10.1016/j.aiepr.2021.07.003.

25. M. U. Azam, I. Belyamani, A. Schiffer, S. Kumar, and K. Askar, "Progress in Selective Laser Sintering Ofmultifunctional Polymer Composites for Strain- and Self-Sensing Applications," *Journal of Materials Research and Technology* 30 (2024): 9625–9646, https://doi.org/10.1016/j.jmrt.2024.06.024.

26. Y. Chunze, S. Yusheng, Y. Jinsong, and L. Jinhui, "A Nanosilica/Nylon-12 Composite Powder for Selective Laser Sintering," *Journal of Reinforced Plastics and Composites* 27, no. 18 (2008): 2133–2142, https://doi.org/10.1177/0731684408094062.

27. B. Chen, R. Davies, Y. Liu, et al., "Laser Sintering of Graphene Nanoplatelets Encapsulated Polyamide Powders," *Additive Manufacturing* 35 (2020): 101363, https://doi.org/10.1016/j.addma.2020.101363.

28. L. Bond, H. Andersson, J. Örtegren, M. Larsson, and M. Engholm, "Electrically Conductive Polymer-Graphene Composite Material for Selective Laser Sintering Additive Manufacturing," *Proceedings of SPIE* 12873 (2024): 1287317, https://doi.org/10.1117/12.3003049.

29. A. M. Vilardell, I. Yadroitsava, W. K. C. Wolf, et al., "Laser Powder Bed Fusion of Polyamide-Composite for Antibacterial Applications: Characterization and Properties," *Materials Today Communications* 31 (2022): 103727, https://doi.org/10.1016/j.mtcomm.2022.103727.

30. M. Marschall, C. Heintges, and M. Schmidt, "Influence of Flow Aid Additives on Optical Properties of Polyamide for Laser-Based Powder

Bed Fusion," *Procedia CIRP* 111 (2021): 51–54, https://doi.org/10.1016/j.procir.2022.08.114.

31. Y.-H. Chueh, X. Zhang, C. Wei, Z. Sun, and L. Li, "Additive Manufacturing of Polymer-Metal/Ceramic Functionally Graded Composite Components via Multiple Material Laser Powder Bed Fusion," *Journal of Manufacturing Science and Engineering* 142 (2020): 051003, https://doi.org/10.1115/1.4046594.

32. Z. Wang, M. Zhou, H. Xiao, and S. Yuan, "Development and Evaluation of Multiscale Fiber-Reinforced Composite Powders for Powder-Bed Fusion Process," *Chinese Journal of Mechanical Engineering: Additive Manufacturing Frontiers* 2, no. 2 (2023): 100079, https://doi.org/10.1016/j.cjmeam.2023.100079.

33. A. C. Lopes, Á. M. Sampaio, and A. J. Pontes, "Development and Characterization of Composite Materials With Multi-Walled Carbon Nanotubes and Graphene Nanoplatelets for Powder Bed Fusion," *Rapid Prototyping Journal* 30, no. 1 (2024): 95–105, https://doi.org/10.1108/RPJ-04-2023-0142.

34. T. Hupfeld, A. Sommereyns, F. Riahi, et al., "Analysis of the Nanoparticle Dispersion and Its Effect on the Crystalline Microstructure in Carbon-Additivated PA12 Feedstock Material for Laser Powder Bed Fusion," *Materials* 13, no. 15 (2020): 3312, https://doi.org/10.3390/ma13153312.

35. A. Mazzoli, G. Moriconi, and M. G. Pauri, "Characterization of an Aluminum-Filled Polyamide Powder for Applications in Selective Laser Sintering," *Materials and Design* 28, no. 3 (2007): 993–1000, https://doi.org/10.1016/j.matdes.2005.11.021.

36. L. Lanzl, K. Wudy, S. Greiner, and D. Drummer, "Selective Laser Sintering of Copper Filled Polyamide 12: Characterization of Powder Properties and Process Behavior," *Polymer Composites* 40, no. 5 (2019): 1801–1809, https://doi.org/10.1002/pc.24940.

37. D. Hui, R. Goodridge, C. Scotchford, and D. Grant, "Laser Sintering of Nano-Hydroxyapatite Coated Polyamide 12 Powders," *Additive Manufacturing* 22 (2018): 560–570, https://doi.org/10.1016/j.addma.2018.05.045.

38. C. Doñate-Buendia, A. Ingendoh-Tsakmakidis, T. Hupfeld, A. Winkel, S. Barcikowski, and B. Gökce, "Production of Bactericidal Powder Suitable for Laser Powder Bed Fusion by Silver Nanoadditivation of Polyamide," *Procedia CIRP* 111 (2022): 47–50, https://doi.org/10.1016/j.procir.2022.08.113.

39. M. Afshari, S. Bakhshi, M. Samadi, and H. Afshari, "Optimizing the Mechanical Properties of TiO_2/PA12 Nano-Composites Fabricated by SLS 3D Printing," *Polymer Engineering and Science* 63 (2022): 267–280, https://doi.org/10.1002/pen.26203.

40. P. Maire, M. Deckert, A. Öchsner, and M. Johlitz, "Influence of UV Irradiation on the Tensile Properties of Titanium Dioxide Composites for the Selective Laser Sintering Process," in *State of the Art and Future Trends in Materials Modelling 2. Advanced Structured Materials* (Springer Nature, 2024), https://doi.org/10.1007/978-3-031-72900-3_5.

41. A. A. Mousa, D. T. Pham, and S. P. Shwe, "Pre-Processing Studies for Selective Laser Sintering of Glass Beads-Filled Polyamide 12 Composites," *International Journal of Rapid Manufacturing* 4, no. 1 (2014): 28–48.

42. R. Seltzer, F. M. de la Escalera, and J. Segurado, "Effect of Water Conditioning on the Fracture Behavior of PA12 Composites Processed by Selective Laser Sintering," *Materials Science & Engineering, A: Structural Materials: Properties, Microstructure and Processing* 528, no. 22–23 (2011): 6927–6933, https://doi.org/10.1016/j.msea.2011.05.045.

43. W. Hui, Y. Hu, Y. Liu, Q. Cai, and W. Zhao, "Development of Thin-Walled Polymer Glass Beads Reinforced 3D Printed Solid Rocket Motors," *Materials Letters* 347 (2023): 134558, https://doi.org/10.1016/j.matlet.2023.134558.

44. J. Z. Liang and R. K. Y. Li, "Mechanical Properties and Morphology of Glass Bead-Filled Polypropylene Composites," *Polymer Composites* 19, no. 6 (1998): 698–703.

45. I. Kletetzka, M. Kosanke, D. Meinderink, et al., "Influence of the Filler–Matrix Adhesion and the Effects of Conditioning on Tensile Properties of Laser-Sintered Parts Built With Polyamide–Glass Bead Dry Blends," *Progress in Additive Manufacturing* 9 (2024): 1039–1048, https://doi.org/10.1007/s40964-023-00501-z.

46. ISO/ASTM 52925:2022, Additive Manufacturing of Polymers—Feedstock Materials—Qualification of Materials for Laser-Based Powder Bed Fusion of Parts, https://www.iso.org/standard/76910.html.

47. ISO 1183-1:2019, Plastics—Methods for Determining the Density of Non-Cellular Plastics—Part 1: Immersion Method, Liquid Pycnometer Method and Titration Method, https://www.iso.org/standard/74990.html.

48. ISO 527-2:2012, Plastics—Determination of Tensile Properties—Part 2: Test Conditions for Moulding and Extrusion Plastics, https://www.iso.org/standard/56046.html.

49. ISO 178:2019, Plastics—Determination of Flexural Properties, https://www.iso.org/standard/70513.html.

50. ISO 180:2023, Plastics—Determination of Izod Impact Strength, https://www.iso.org/obp/ui/#iso:std:iso:180:ed-5:v1:en.

51. ISO 179-1:2023, Plastics—Determination of Charpy Impact Properties—Part 1: Non-Instrumented Impact Test, https://www.iso.org/standard/84393.html.

52. B. Van Hooreweder, F. De Coninck, D. Moens, R. Boonen, and P. Sas, "Microstructural Characterization of SLS-PA12 Specimens Under Dynamic Tension/Compression Excitation," *Polymer Testing* 29, no. 3 (2010): 319–326, https://doi.org/10.1016/j.polymertesting.2009.12.006.

53. S. Rosso, R. Meneghello, L. Biasetto, et al., "In-Depth Comparison of Polyamide 12 Parts Manufactured by Multi Jet Fusion and Selective Laser Sintering," *Additive Manufacturing* 36 (2020): 101713, https://doi.org/10.1016/j.addma.2020.101713.

54. Y. Liu, L. Zhu, L. Zhou, and Y. Li, "Microstructure and Mechanical Properties of Reinforced Polyamide 12 Composites," *Rapid Prototyping Journal* 25, no. 6 (2019): 1127–1134, https://doi.org/10.1108/RPJ-08-2018-0220.

55. B. Özbay Kısasöz, İ. E. Serhatlı, and M. E. Bulduk, "Selective Laser Sintering Manufacturing and Characterization of Lightweight PA12 Polymer Composites With Different Hollow Microsphere Additives," *Journal of Materials Engineering and Performance* 31, no. 5 (2022): 4049–4059, https://doi.org/10.1007/s11665-022-06780-0.